Estuarine, Coastal and Shelf Science 220 (2019) 220–231

Contents lists available at ScienceDirect

Estuarine, Coastal and Shelf Science

journal homepage: www.elsevier.com/locate/ecss

Spatial and temporal variation in chlorophyll *a* concentration in the Eastern China Seas based on a locally modified satellite dataset

Qiang Hao[a,b,*], Fei Chai[b,d], Peng Xiu[c], Yan Bai[b], Jianfang Chen[a], Chenggang Liu[a,b], Fengfeng Le[a], Feng Zhou[b]

[a] Key Laboratory of Marine Ecosystem and Biogeochemistry, State Oceanic Administration, Second Institute of Oceanography, Ministry of Natural Resources, Hangzhou, 310012, China
[b] State Key Laboratory of Satellite Ocean Environment Dynamics, Second Institute of Oceanography, Ministry of Natural Resources, 36 Baochubei Road, Hangzhou, 310012, China
[c] State Key Laboratory of Tropical Oceanography, South China Sea Institute of Oceanology, Chinese Academy of Sciences, Guangzhou, 510301, China
[d] School of Marine Sciences, University of Maine, Orono, 04469, USA

ARTICLE INFO

Keywords:
Chlorophyll *a*
Satellite
Eastern China seas
Phytoplankton
Biogeochemical cycle
OC-CCI

ABSTRACT

Satellite chlorophyll *a* (Chl) is an essential parameter for large-scale studies on changes in the marine ecosystem and biogeochemistry. However, in the eastern China seas (ECSs), the coexistence and interaction of turbid and clear water pose challenges to the application of standard satellite Chl products to studies on phytoplankton dynamics. Based on the empirical modification of the OC-CCI (Ocean Colour Climate Change Initiative) standard products, we herein provide a locally modified chlorophyll *a* (LMC) dataset and compare the large-scale Chl distributions with satellite and in-situ Chl datasets. Compared with standard Chl, LMC has a higher correlation with in-situ data (R^2 = 0.58) and lower Bias (0.08) and is more consistent with the ship-measured Chl distributions. Using the LMC dataset, we analyzed the climatological Chl distributions in the ECSs and classified the Chl annual cycles into four types. Our results suggest that high Chl patterns not only rely on nutrient supply, but also relate to light conditions controlled by vertical mixing and suspended matter. The different Chl annual cycles are mainly caused by differences in the duration and range of nutrients and light limitation, and thus their distributions tend to vary with water depth. We believe that this work presents a more accurate dataset in the ECSs and can improve the understanding of local biogeochemical cycles.

1. Introduction

Satellite chlorophyll products can intuitively and efficiently reflect phytoplankton dynamics in the ocean and are commonly used in studies of marine ecosystem and biogeochemical cycle (Falkowski et al., 1998; Reygondeau et al., 2013). As a major phytoplankton light-absorption pigment and proxy for phytoplankton standing stock, chlorophyll *a* concentration (Chl) can be calculated by bio-optic algorithms and water-leaving signals received by ocean-color sensors. Standard satellite Chl products, which are most frequently used, are usually derived from blue-green ratio bio-optic algorithms and water-leaving signals corrected by the NIR (near-infrared) atmospheric correction. Because both the bio-optic and atmospheric correction algorithms were developed in clear water, the accuracy of standard Chl products in turbid water is often questioned (IOCCG, 2000; Gregg and Casey, 2004).

The eastern China seas (ECSs), including the Bohai Sea (BH), Yellow Sea (YS), and East China Sea (ECS), are the largest marginal seas in the Northern Hemisphere, and the most productive areas of East Asia, serving as important fishing grounds (Ning et al., 1995; Tang, 2012). ECSs have the broadest continental shelf in the world and the terrain slopes from northwest to southeast (Fig. 1). In coastal and inner shelf areas, turbid and eutrophic waters are common, mainly due to massive terrestrial input and strong vertical mixing. The rivers around the ECSs transport about 1.4×10^{12} m^3 of discharge water and 1.9×10^9 t of suspended sediment per year into the coastal regions (Yang et al., 2003; Gao et al., 2017). These river inputs have high seasonal and annual variability because of rainfall and anthropogenic activities, and diffusion depends on the interaction of discharge water, coastal currents, and Ekman transport (Liu et al., 2006; Song et al., 2016). In shallow water, because of strong winds, waves, and tidal currents, sediments are

* Corresponding author. Key Laboratory of Marine Ecosystem and Biogeochemistry, Second Institute of Oceanography, Ministry of Natural Resources, Hangzhou, 310012, China.
E-mail address: haoq@sio.org.cn (Q. Hao).

https://doi.org/10.1016/j.ecss.2019.01.004
Received 19 May 2018; Received in revised form 30 December 2018; Accepted 8 January 2019
Available online 09 January 2019
0272-7714/

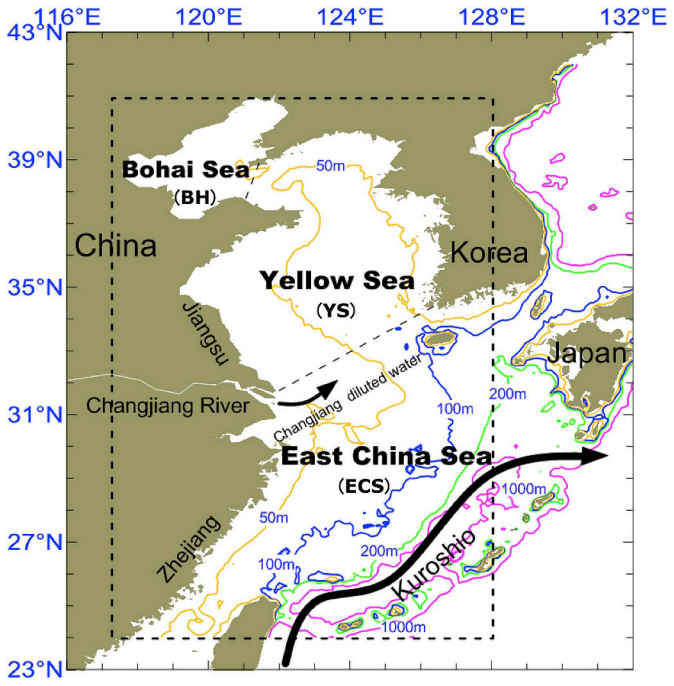

Fig. 1. Location and bathymetry of the eastern China seas, including the Bohai Sea (BH), Yellow Sea (YS), and East China Sea (ECS), with the study area marked by a dashed-line rectangle.

easily stirred and suspended, while upper nutrients are quickly re-supplied from the bottom, especially during winter (Chen, 2009; Bian et al., 2013). In the eastern and southern ECS, the Taiwan Warm Current (TWWC) and Kuroshio (KS) dominate, with high transparency but low nutrient levels in surface water. Driven by the Asian monsoon, the clear and oligotrophic surface waters of the TWWC and KS intrude and occupy the shelf in summer but weaken in winter (Ichikawa and Beardsley, 2002). The surface water has relatively high temperatures and high salinity; hence, it controls the strength of the thermocline and nutrient supply to marine phytoplankton (Chen et al., 2004; Zhang et al., 2007; Wang et al., 2016). On a large scale, water turbidity and nutrients levels, driven by interactions between coastal and oligotrophic masses, significantly impact phytoplankton dynamics and the accuracy of satellite ocean color products (Ning et al., 1998; Kiyomoto et al., 2001; Gong et al., 2003).

The standard satellite Chl product is often reported to be overestimated due to high turbidity in the ECSs (Kiyomoto et al., 2001; He et al., 2013a; Yamaguchi et al., 2013). In turbid water, strong backscattering effected by high non-algae suspended matter (SPM) concentration causes apparent increase of water-leaving reflectance at green and red light bands. While water-leaving reflectance at blue light band increases quite small compared to that at longer wavelength, because of the strong absorption caused by abundant detritus and colored dissolved organic matter (CDOM). Thus, it decreases the blue-green bands reflectance ratio, and leads to the overestimation of Chl concentration by the OCx algorithms (Gohin et al., 2002; He et al., 2012, 2013b). In the ECSs, the accuracy of the OC3 or OC4 algorithms in the shallow, turbid water (e.g., YS and BH) is far lower than in that in clear water (Case 1 water) (Siswanto et al., 2011). Standard Chl can reach 500% overestimation in very turbid areas (Ahn et al., 2001), and the Chl-based satellite net primary production can also be several times higher than the in-situ isotope tracing results (Ning et al., 1995) in the BH, YS, and parts of the ECS. There have been efforts to develop bio-optical Chl algorithms for turbid water (Case 2 water). For both clear and turbid water, these algorithms cannot be applied throughout the ECSs. Siswanto et al. (2011) optimized a two-band Chl algorithm for turbid water in the YS and ECS. This algorithm and the standard Chl algorithm could be interchangeably applied, referring to a 555 nm normalized water-leaving radiance (nLw555) in water with different levels of clarity, to obtain estimates with higher precision. Yamaguchi et al. (2013) combined OC4 and Siswanto's two-band algorithm in a step-smooth method to develop a new Chl database, providing more accurate Chl images than those of standard products. Besides bio-optic algorithms, another major error source is the standard atmospheric correction algorithm. It usually over-corrected the short wavelength band water reflectance in turbid water and thus led to errors in satellite products (Wang, 2007). Chen et al. (2014) reported on the combination of different atmospheric correction algorithms, which could improve the quality of remote-sensing reflectance in the coastal regions of the ECSs yielding higher estimation accuracy in summer, but lower accuracy in winter.

In the past decades, many studies have reported that the phytoplankton biomass in the ECSs exhibits dramatic spatial-temporal variation, with complex control mechanisms (Ning et al., 1995, 1998; Gong et al., 1996, 2003; Chen et al., 2004). Ship-measured results show that Chl can change by around four orders of magnitude in the ECSs. Extremely high Chl was recorded in the coastal area and low Chl usually appeared at the center of YS, TWWC, and KS. The spatial distribution of phytoplankton, which generally decrease with increasing water depth, are clearly associated with nutrient distribution. Ning et al. (1995, 1998) reported that the large-scale distribution of Chl is dominated by interactions between coastal water and Kuroshio water masses, which are the two major nutrient sources in the ECSs (Zhang et al., 2007). Empirical correlation analysis has shown that other factors, such as temperature, salinity, suspended matter and zooplankton are correlated with Chl in different contexts, suggesting that phytoplankton dynamics may be controlled by multiple factors in different regions (Sun and Su, 2012; Liu and Wang, 2013; Song et al., 2014). On the other hand, both large-scale ship-based surveys and remote sensing results have shown that Chl cycles varied in the BH, YS, and ECS (Ning et al., 1995, 1998; Tang et al., 1998; Tang, 2006), suggesting that there may be several types of Chl seasonal variation in the study area (Fu et al., 2009; Yamaguchi et al., 2012). However, due to overestimation in highly turbid water, phytoplankton dynamics derived from satellite Chl products often contrast with ship-based observations. Short-term phytoplankton blooms make it difficult to compare the Chl distributions from different sources. Although a large amount of ship-measured data has been accumulated, climatological Chl distributions are rarely reported in the ECSs, so annual Chl cycles and related control processes are not completely understood.

In this study, we aim to reveal the climatological distributions and annual cycles of phytoplankton in the ECSs using a remote sensing approach. Herein, we present a new, locally modified Chl (LMC) dataset that is based on the empirical relationship between water reflectance and the error of standard Chl. This LMC was verified by large-scale in-situ data and can provide more reasonable Chl spatio-temporal variations than the standard Chl in the study area. We also compared monthly climatological Chl distributions derived from different sources, and divided Chl annual variation into different types based on spectral clustering. Finally, the major factors controlling phytoplankton dynamics were analyzed, and the related physicochemical processes were discussed for different Chl annual cycles.

2. Materials and methods

2.1. Satellite and in-situ dataset

Satellite data were obtained from the Ocean Colour Climate Change Initiative dataset (OC-CCI, Version 2.0) of the European Space Agency (ESA, http://www.esa-oceancolour-cci.org). The OC-CCI dataset is merged from MODIS, SeaWiFS (Sea-viewing Wide Field-of-view Sensor), and MERIS (Medium Resolution Imaging Spectrometer) data. The resolution is 4 km × 4 km and coverage runs from 1998 to 2013.

Standard Chl was directly derived from the OC-CCI Chl daily product, calculated by the OC4 algorithm (O'Reilly et al., 2000) and OC-CCI remote-sensing reflectance (Rrs) products. For OC-CCI Rrs products, MODIS and MERIS Rrs data were band-shifted to SeaWiFS bands when necessary and then merged with SeaWiFS Rrs data. Thus OC-CCI v2.0 ocean color products can be regarded as being the same as the original SeaWiFS products. The normalized water-leaving radiance at 555 nm (nLw555) was used to indicate water turbidity, following Siswanto et al. (2011). Daily nLw555 data were calculated by OC-CCI Rrs555 products (nLw555 = F_0 × Rrs555, where F_0 is the extraterrestrial solar irradiance for the 555 nm band in SeaWiFS, and Rrs555 is the daily remote-sensing reflectance at the 555 nm wavelength). Eight-day, monthly, and 16-year averages were calculated based on daily products. All data processing (including local modification) was carried out in BEAM 5.0 software.

The in-situ Chl used for establishing the locally modification derives from the SeaDASS (SeaWiFS Bio-optical Archive and Storage System, seabass.gsfc.nasa.gov) and LMEB (Key Laboratory of Marine Ecosystem and Biogeochemistry, Ministry of Natural Resources, China) in-situ database, which come from varies projects carried in the YS and ECS from 1984 to 2013. In the present study, we only collected the surface Chl (sampling depth ≤ 3 m) by using extracting fluorescence method. The daily match-up data are from the in-situ Chl that have corresponding satellite data in the same pixel (4 km × 4 km) and on the same day. The 8-d match-up data are from the in-situ data observed during the period of their corresponding 8-d average satellite data in the same pixel. To avoid the impact of extreme values, we used the dataset in which the ratio of satellite Chl to in-situ Chl is between 0.1 and 10 to develop a locally modified algorithm, following the method of Johnson et al. (2013). This results in a 2% and 4% loss of daily and 8-d match-up data, respectively. Finally, there are 278 and 802 stations that could match the daily and 8-d products, respectively, and that were used to develop the local modification (Fig. 2). Furthermore, an independent in-situ Chl dataset, including 346 daily matched stations, was used to verify the locally modified Chl results. This dataset comes from "The China Sea Environment Integrated Survey and Assessment Project", which was carried in 2006–2007 and its survey area covered BH, YS and ECS. In this project, Chl was also measured by extracting fluorescence method and the sample treatment procedures are unified in all stations. Using this independent dataset for our model verification can help to reduce potential data bias due to different in-situ Chl data sources.

In order to reveal the difference between satellite and in-situ Chl, we mapped in-situ Chl distributions in four seasons using integrated ship-measured surface Chl data collected in January, April, July, and October in SeaBASS and LMEB dataset. We did not use a three-month mean for each season, because the difference between April and May is large. Since in-situ Chl data were measured in different years, on different cruises, and at different stations, they first needed to be consolidated into an integrated ship-measured dataset. We divided the study area into 0.25° × 0.25° bins, and calculated the averaged in-situ data in each bin in a month. The nearest neighbor method was adopted for interpolation and contours were drawn with Surfer 11 software.

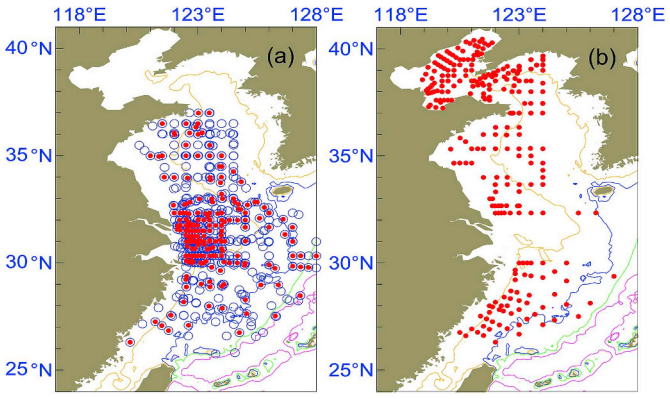

Fig. 2. Station distributions of **(a)** in-situ Chl dataset used for establishing the locally modification, and **(b)** an independent in-situ Chl dataset used for verifying the locally modified Chl results. Red dots are Chl stations matched with daily Chl data, and open blue circles denote Chl stations matched with 8-day Chl data. (For interpretation of the references to color in this figure legend, the reader is referred to the Web version of this article.)

2.2. Local modification of standard Chl

Overestimation of the standard Chl in the ECSs is mainly attributed to the high water turbidity (Ahn et al., 2001; Shi and Wang, 2012; Siswanto et al., 2011). The high water turbidity mainly causes 1) the increase of water-leaving reflectance at green and red light bands; 2) the underestimation of the water-leaving reflectance at blue light band by using the NIR atmospheric correction method (He et al., 2012). These changes in reflectance lead to blue-green bands ratio decrease and overestimation in standard Chl products (IOCCG, 2000; Siegel et al., 2000; Gohin et al., 2005). Therefore, in this study, we applied nLw555, which usually indicates the water reflectance induced by non-algae matter, to correct the error of standard Chl by using an extensive in-situ dataset. First, we used an 8-d match-up dataset to establish an empirical correlation between nLw555 and the standard Chl error and described it with a fourth-order polynomial function. Second, the daily match-up dataset was used for further modification by the type II linear regression. The function employed for the local modification of standard Chl is described below (Eq. (1)) and the development procedures are described in detail in Appendix B.

$$C_{LMC}=(C_{OC}/f\ )^{1.11} \tag{1}$$

$$f = 10^{(-0.4122L^4+0.4101L^3-0.3810L^2+0.2242L+0.1929)}$$

where C_{LMC} and C_{OC} are LMC and the standard Chl, respectively, and the units are $mg{\cdot}m^{-3}$. L is Log_{10}(nLw555) and the unit of nLw555 is $mW{\cdot}cm^{-2}{\cdot}\mu m^{-1}{\cdot}sr^{-1}$.

2.3. Statistical analysis

Standard major axis type II linear regression was applied to compare and evaluate the matched datasets. This method is applied when two variables to be compared are independent but have uncertainties (Sokal and Rohlf, 1995). As the natural distribution of Chl is lognormal (Gregg and Casey, 2004), error estimation was also based on logarithmically normalized data. The root mean square log error (RMS_{log}) between the remote sensing and in-situ datasets is defined as follows:

$$RMS_{log} = \sqrt{\frac{\sum [Log_{10}(S) - Log_{10}(I)]^2}{n}} \times 100 \tag{2}$$

and the average difference (Bias) is defined as follows:

$$Bias = \frac{\sum [Log_{10}(S) - Log_{10}(I)]}{n} \times 100 \tag{3}$$

where S indicates remote sensing data, I indicates in-situ data, and n is the number of samples. RMS_{log} is an estimate of the error of the remote sensing dataset. The average difference is an estimate of the Bias, and the coefficient of determination (R^2) from correlation analysis indicates the covariance between the remote sensing dataset and in-situ observations.

2.4. Spectral clustering analysis

To distinguish different types of annual variation in Chl, we applied spectral clustering to analyze the LMC dataset. Spectral clustering is a popular clustering algorithm used widely in pattern recognition that

treats data clustering as a graph partitioning problem without making any assumptions on the form of data clusters (von Luxburg, 2007). The essence of a spectral clustering algorithm is to map a high-dimensional space into a low-dimensional space, obtaining a more compact dataset with similar distribution (Ng et al., 2001). Thus, spectral clustering can be solved efficiently by standard linear algebra software, and usually outperforms traditional clustering algorithms such as the K-means algorithm. In this study, the annual variation in Chl is described as an "annual variation curve" composed of 12 monthly mean Chl values. By conducting spectral clustering analysis on curves with different shapes, we obtained clusters of Chl annual variation. Firstly, matrices with 12 columns were created, where the number of rows is equal to the number of valid pixels in each image (not excluding cloud and land pixels). The 12 columns in the matrices correspond to climatological monthly mean Chl concentrations from January to December. Secondly, all data were normalized following Shi and Malik (2000) to avoid errors induced by maximum and minimum values. Then, we followed von Luxburg (2007) in choosing a normal k-nearest neighbor similarity graph, set different cluster numbers, and carried out cluster analysis using the normalized dataset and the spectral cluster tool in Matlab. Finally, we compared the distributions of cluster results derived by different cluster numbers, and blanked the cluster results to the west of the Ryukyu Islands. We found that the optimum cluster number is four.

3. Results

3.1. Verification of locally modified Chl

We compared the accuracy of LMC and standard Chl using an independent daily match-up in-situ dataset. Fig. 3a shows that despite correlation between the log-normalized daily standard Chl and in-situ data (R^2 = 0.49), most data pairs are located above the 1:1 line, and RMS_{log} and Bias are quite high (RMS_{log} = 46%, Bias = 0.35). This suggested that the standard Chl leads to overestimation of Chl in the ECSs and the error exceeds the 35% error allowance (IOCCG, 2000) in the global seas. Fig. 3b shows that LMC has a higher correlation (R^2 = 0.58) with in-situ Chl than with the standard Chl. More importantly, the Bias and RMS_{log} are reduced to 0.08 and 32%, respectively, and the data pairs are evenly distributed near the 1:1 line. These results suggest that the standard Chl has significant overestimation in the ECSs. The local modification, which is based on nLw555, can effectively reduce the error of standard Chl in the study area.

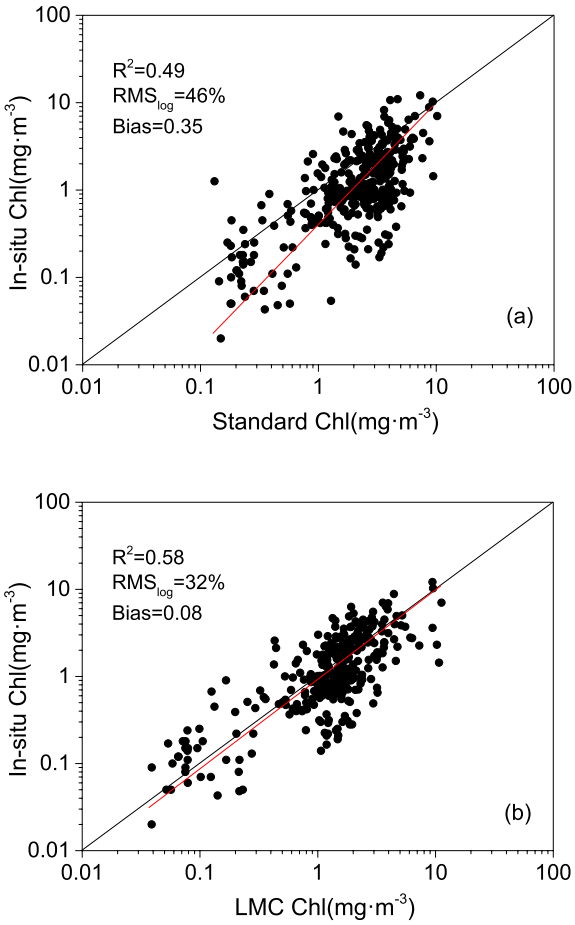

Fig. 3. Comparison between log-normalized daily matched satellite data and in-situ data: (**a**) Standard Chl versus in-situ Chl, and (**b**) locally modified Chl (LMC) versus in-situ Chl. The black line is Y:X = 1:1, and the red line shows a type II linear regression. (For interpretation of the references to color in this figure legend, the reader is referred to the Web version of this article.)

3.2. Distributions of ship-measured and standard Chl, and LMC

Fig. 4 presents the climatological distributions from ship-measured Chl, standard Chl, and LMC. Our results show that LMC is consistent with the ship-measured results and the standard Chl is significantly different from both LMC and ship-measured Chl. The spatial variations of integrated ship-measured Chl are greatest in summer and least in winter (Fig. 4a). The high Chl ($> 2\,mg{\cdot}m^{-3}$) areas are mainly concentrated in the continental shelf, the coastal zone, and the estuary, corresponding to the well-known seasonal phytoplankton blooms. The low Chl ($< 0.2\,mg{\cdot}m^{-3}$) areas are mainly located in the continental shelf and open sea areas of the ECSs, coupling with the oligotrophic water masses, such as the KS and TWWC. While the standard Chl is similar to the ship-measured result in summer, it is significantly higher than the integrated ship-measured Chl in the other three seasons (Fig. 4b). The overestimation of the standard Chl mainly occurs in areas in which the water depth is less than 100 m; it is most serious on January, but reduces on July. These standard Chl images create an illusion that the high Chl patterns always appear inshore throughout the year and the offshore blooms are not apparent.

LMC is significantly lower than the standard Chl and its high and low patterns' distributions match the ship-measured results very well (Fig. 4c). The differences of LMC and standard Chl are also greatest in the shallow waters and least in the open sea. Similar to the ship-measured Chl, the spatial distribution of the LMC is moderate in winter and shows significant dynamics in spring and summer. The inshore and offshore blooms can be clearly distinguished by the LMC images, which depict the evolution process of high Chl patches in the ECSs. The high Chl ($> 2\,mg{\cdot}m^{-3}$) patches first appear at the center of the YS and in the inner shelf of the ECS in April, but do not occur in very shallow water, which reflect typical continental shelf spring blooms (Fu et al., 2009). In May, the high Chl patterns disappear in the shelf zone but gradually concentrate in the estuaries and coastal zones (e.g., the Changjiang Estuary, Zhejiang coast, and the west coast of the Korean Peninsula), which indicates that the summer coastal blooms are induced by discharge water and coastal upwelling (Ning et al., 1998). These high Chl patches near the coast and estuary increase to a maximum in July and subside in October. In contrast, the low Chl ($< 0.2\,mg{\cdot}m^{-3}$) areas expand in summer and shrink in winter, and reflect more details of the oligotrophic water features. Note that the satellite distribution was smoothed by multi-year averaged data, thus the high and low Chl patterns in LMC were not as significant as the ship-measured results.

3.3. Classification of Chl annual cycle

As shown in Fig. 5, the annual cycles in Chl can be classified into four types in the ECSs: (1) summer bloom (SB), with the highest Chl occurring in summer and the lowest in winter; (2) spring and autumn bloom (SAB), where high values of Chl occur in spring and autumn and

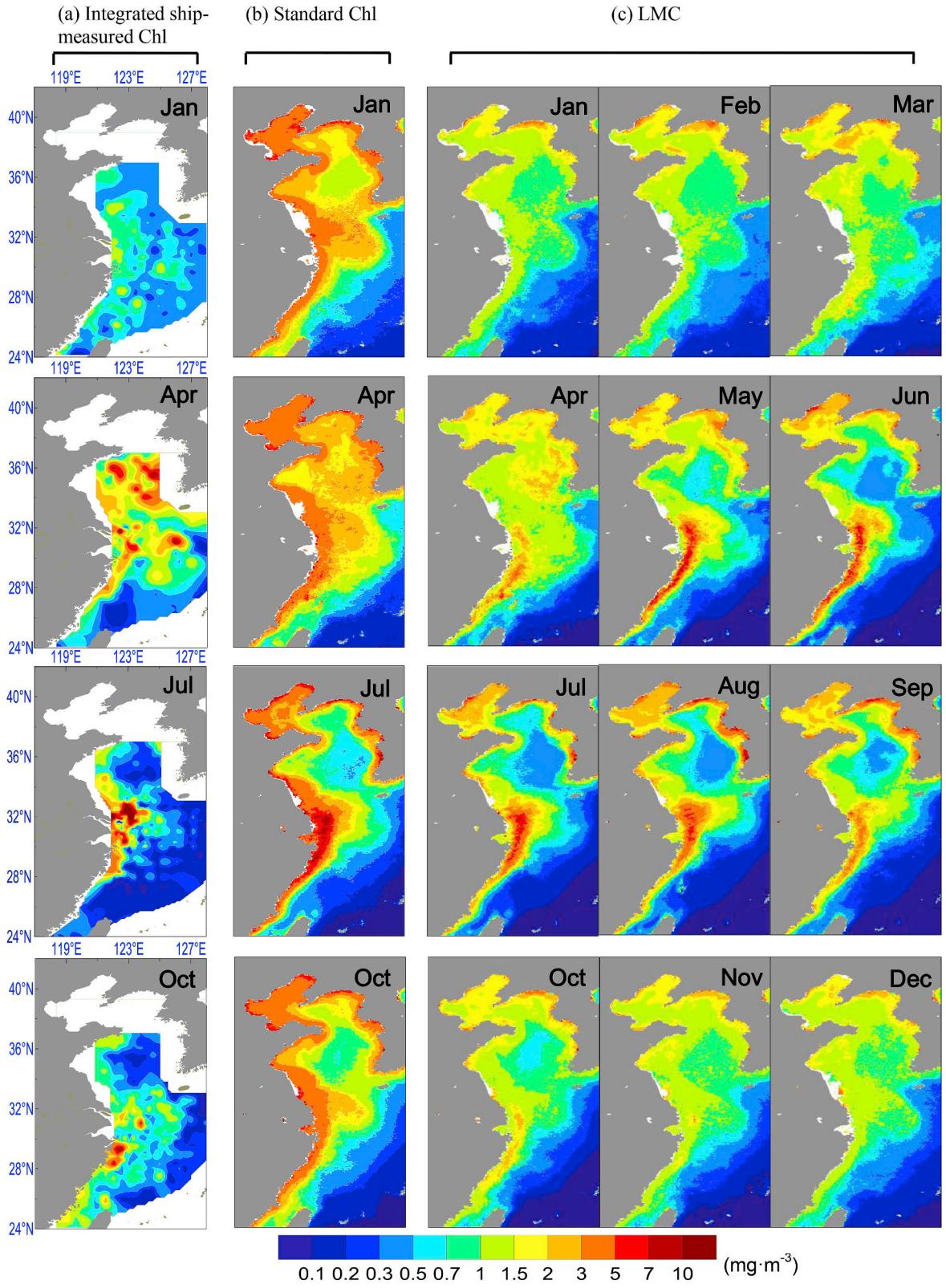

Fig. 4. Distributions of **(a)** the integrated ship-measured Chl, **(b)**16-year averages of monthly standard Chl in four seasons, and **(c)**16-year averages of monthly LMC.

low values occur in summer and winter; (3) early spring bloom (ESB), where high values of Chl occur in March and April, and low values occur in summer and autumn; and (4) low Chl (LC), where Chl is quite low and the seasonal variation is not significant. Chl concentration levels for the four types are in the order of SB > SAB > ESB > LC. The spatial distribution of Chl annual cycles seems to change with isobaths. The SB type appears in the BH, the coastal water of YS, an area outside the Changjiang River Estuary, where water depth is less than 50 m, and both sides of 50 m isobaths in the coastal area of Zhejiang Province. The SAB type is mainly located in the central YS and the central ECS shelf with water depth between 50 m and 100 m. The ESB zone covers the area outside the ECS shelf, with water depth less than 200 m. The LC

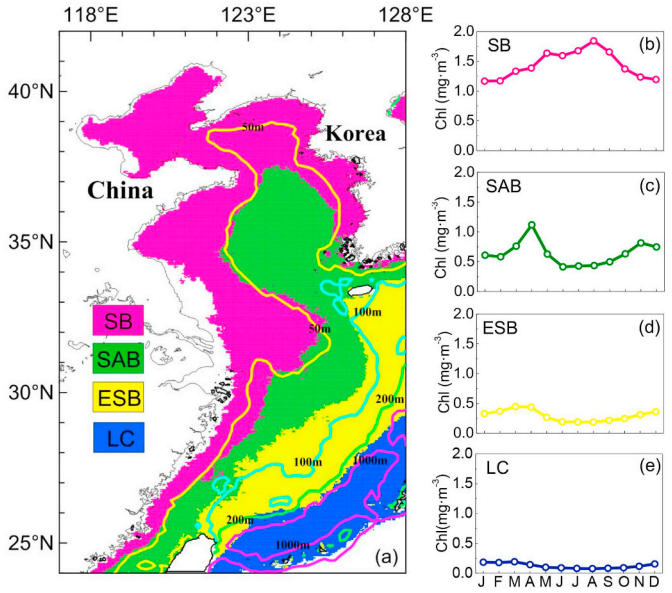

Fig. 5. The different Chl annual cycle types in the Eastern China Seas: (**a**) Distribution of four Chl annual cycle types with bathymetry: summer bloom (SB), spring and autumn bloom (SAB), early spring bloom (ESB), and low chlorophyll (LC); (**b-e**) monthly-mean Chl variations for different types.

type is located in the area outside the 200 m isobaths, which is dominated by the KS.

4. Discussion

4.1. Comparison between LMC, standard Chl and previous studies

Since the 1980s, several investigations covering the BH, YS, and ECS have provided the framework for large-scale phytoplankton dynamics (Fei et al., 1991; Lv et al., 1999; Fu et al., 2009; Gong et al., 2003; Ning et al., 1995; Sun and Su, 2012; Tang, 2006; Zhu et al., 1993). In general, variations in phytoplankton biomass and primary productivity in the ECSs are mainly controlled by the "bottom-up processes" (Ning et al., 2000), the high Chl mainly occurs in the summer half of year (spring or summer) and the low value always appears in winter. The annual Chl levels in the BH, YS, and ECS are usually between 0.5 and 2 $mg{\cdot}m^{-3}$. The average annual Chl in the entire ECSs is about 1 $mg{\cdot}m^{-3}$ (Appendix A; Table 2). Our results show that the standard Chl is much higher than the ship-measured results, and the overestimation is more significant in winter and in shallow waters (Fig. 4). Overestimation of the standard Chl in the ECSs has been previously highlighted and is originally attributed to high water turbidity (Kiyomoto et al., 2001; Ahn et al., 2001; Shi and Wang, 2012; Siswanto et al., 2011). In the ECSs, due to the wind-induced strong mixing and subtidal currents, sediment becomes easily re-suspended and can be transported further in winter (Qiao et al., 2016), which leads to expansion of the high SPM area and a significant increase in water reflectance. In summer, sediment suspension and transportation are inhibited due to the strong seasonal thermocline and the barrier effect of fronts and shelf circulations (Dong et al., 2011; Bian et al., 2013), which causes the decrease in water turbidity. These processes result in significant seasonal variations in sea surface reflectance and relative higher overestimation of standard Chl in winter (Appendix A; Fig. 2), especially in the shallow water areas, such as in the BH. In these shallow water areas, standard Chl are much higher during the winter half year, resulting in inverse seasonal variations compared to the LMC and previous ship-measured results.

LMC is more consistent with ship-measured Chl distribution compared to standard Chl. In the BH, the YS and the ECS, the annual average LMC are 1.91, 1.27 and 0.64 $mg{\cdot}m^{-3}$, respectively, which is close to the results of previous large investigations (Ning et al., 1995; Sun and Su, 2012). The high Chl in LMC appears in spring and summer and their patterns are also highly consistent with the previous description of phytoplankton blooms (Chen et al., 2004; Fu et al., 2009). These results suggest that it is feasible to correct standard products using the empirical relationship between the satellite Chl error and water reflectance in the study area, although there is no improvement in bio-optical and atmospheric correction algorithms in our local modification. Yamaguchi et al. (2013) and Shi and Wang (2012) reported corrected Chl distributions in the ECSs using improved bio-optical algorithms and atmospheric correction algorithms, respectively. Our results show that both LMC and the integrated ship-measured Chl distribution are closer to the results of the improved bio-optical algorithm than those of the improved atmospheric correction. This is because the error of standard Chl mainly comes from the bio-optical algorithm (IOCCG, 2000; Volpe et al., 2007) in the high reflectance water, and the error caused by atmospheric correction is more likely to have a higher bias (Shi and Wang, 2012). Improving the applicability of satellite products over clear and turbid water is still a very complex issue. It not only requires greater knowledge of the bio-optical properties of water, but also relies on advances in bio-optical algorithms, atmospheric correction, the combination of different algorithms, and the performance of ocean color sensor (Blondeau-Patissier et al., 2014; Han et al., 2016).

4.2. The fate of high Chl events

In the ECSs, the occurrence of phytoplankton blooms were reported to be associated with water stability and SPM variations (Fu et al., 2009; Zhu et al., 2009; Yamaguchi et al., 2013; Zhou et al., 2013). This is because both water stability and SPM can affect the light exposure to phytoplankton cells and thereby indirectly control phytoplankton growth when nutrient supply is not a limiting factor. For surface phytoplankton, cell exposure to light energy is dominated by mean light energy (LE) in the mixed layer (Nicklisch et al., 2008), rather than by water surface light energy. As shown in Eq. (4), daily LE can be calculated from the daily sea surface light energy (I_0, $Einstein{\cdot}m^{-2}{\cdot}d^{-1}$), MLD (m), and light attenuation (K, m^{-1}). MLD is associated with water stability and K is controlled by SPM. When I_0 is stable, LE is controlled by both MLD and K, and its variability will be sensitive to the parameters that change more quickly.

$$LE = \frac{I_0}{MLD \times K} \times [1 - \exp(-MLD \times K)] \quad (4)$$

In the central YS, SPM concentration was reported changing by a factor of 1–3 during the early spring period, but changes in MLD are not significant and thermoclines are very weak during the same time (Han, 2008; Huang et al., 2010; Hao et al., 2012; Yamaguchi et al., 2013). This implies that the variability in LE is mainly influenced by SPM rather than MLD, and SPM is therefore probably more important to phytoplankton growth during the bloom period. Our results show that, in April, the high Chl (> 2 $mg{\cdot}m^{-3}$) events rarely occur in very shallow YS coastal water, which has the highest nutrients, highest SPM, and the lowest MLD (Wang et al., 2003, 2013; Shi and Wang, 2010). This suggests that YS spring bloom might be more sensitive to SPM. Moreover, LMC images also show that the locations of high Chl patterns in the ECS are closer to the coast than those in the YS. This may be related to the Zhejiang coastal upwelling fronts and Changjiang Estuary fronts in spring. These fronts form in March–April, and MLD will decrease quickly offshore of these fronts (Pan et al., 1987; Huang et al., 2010). The decrease in MLD will benefit the accumulation of phytoplankton and increase LE, even in high SPM, thereby likely promoting phytoplankton blooms in the coastal front zones of ECS. LE is essential for understanding phytoplankton outbreaks (especially in harmful algae blooms) in coastal eutrophic area, but its spatio-temporal variations have rarely been observed in the ECS. Elucidation of the variations in

LE requires further efforts with respect to the combination of in-situ and remote sensing time-series observations, particularly in terms of obtaining more details of SPM and MLD variations.

The duration of high Chl patterns varies because of different nutrient supply mechanisms. In the continental shelf area, nutrient supply mainly relies on the up-mixing of subsurface water. The seasonal thermocline, usually forming in late spring, blocks nutrient supply and thus leads to surface nutrient depletion after spring bloom (Fu et al., 2009; Wang et al., 2003). Jin et al. (2013) reported that nutrients in the upper layer of the central YS can only support phytoplankton blooms for two weeks in April. Our results confirm that the continental spring bloom quickly subside after April, since the nutrient limitation probably begins in late spring. In contrast, the coastal upwelling and terrestrial input provide continued nutrient supply (especially phosphate) to the upper layer, although there is an obvious thermocline during the summer half of the year (Wong et al., 1998; Wang and Wang, 2007; Hu and Wang, 2016). These sustained nutrient supplements allow the high Chl to persist from April until October in these areas (Fig. 4c). However, the decline of high Chl in coastal region is not due to phosphate depletion in autumn, because vertical mixing increases the sea surface phosphate concentration (Wang et al., 2003). The subside of high Chl patterns might be related to increase of water turbidity and vertical mixing, which were driven by steering of coastal currents and increasing of the eastern Asian monsoon in autumn (Ning et al., 1998; Li et al., 2016). These processes will lead to decrease of LE and thus probably inhibiting the phytoplankton growth. Ning et al. (2004) suggested that the phytoplankton primary productivity is controlled by the light conditions in eutrophic coastal water and phytoplankton biomass should quickly decrease when light limitation occurs.

4.3. Types of annual cycle in Chl

Unlike previous studies (Fu et al., 2009; Gong et al., 2003; Ning et al., 2000, Tang, 2006), we classified annual cycles of chlorophyll in the ECSs into four types (Fig. 5). These types and their locations are useful for understanding the differences among previous regional studies, describing seasonal Chl variations in the ECSs and revealing why Chl seasonal cycles are different in the BH, YS, and ECS (Sun and Su, 2012). To understand these different annual Chl cycles, we compared the area-averaged LMC and the corresponding basic environmental factors that controls phytoplankton growth (Falkowski and Raven, 2007) in the SB, SAB, ESB, and LC regions, including sea surface temperature (SST), the concentration of major nutrients (DIN, PO_4, SiO_3), and LE. These data were derived from satellite databases and eight cruises ship-measured results in the PN section, which extends from the Changjiang Estuary to the Ryukyu Islands and crosses the four regions (see Appendix B).

As shown in Fig. 6a and b, in the SB region, the Chl variation is consistent with LE and SST rather than with nutrients. Due to the input from terrestrial sources and shallow water mixing, all concentrations of N/P/Si are much higher than the limiting thresholds (DIN = 1 μmol·dm^{-3}, PO_4 = 0.1 μmol·dm^{-3} and SiO_3 = 2 μmol·dm^{-3}, suggested by Justić et al., 1995), which suggests there is no nutrient limitation in the SB region. LE in winter is only 1.7 Einstein·m^{-2}·d^{-1}, which is significantly lower than the reported saturated irradiance for diatoms at similar temperatures (Foy and Gibson, 1993; Li et al., 2017). This suggests that light probably limits the diatom blooms in winter. In addition, the highest correlation (R^2 = 0.92, data not shown) between SST and Chl appears in the summer half year in the SB region. Temperature usually synergizes with light and nutrients because it controls the activity of the enzymes in the phytoplankton cell but does not directly control the input of material and energy (Falkowski and Raven, 2007). Thus, phytoplankton growth might be dominated by temperature during periods when both light and nutrient are not limited. In the SAB region (Fig. 6b), nutrients levels decrease because of the stronger seasonal thermocline, lower contributions by terrestrial inputs, and greater influences of oligotrophic waters (Hao et al., 2012; Ning et al., 1998). DIN is lower than the threshold in summer and LE is still very low in winter. Chl peaks occur in April and November due to relatively high nutrient and LE levels, which implies that the high phytoplankton growth rate is likely caused by the best balance of nutrient and light. In the ESB region, nutrient levels decease further, and the PO_4 limitation begins in April. Correspondingly, the Chl level peaks in March, but decreases in April. In the LC region, which is dominated by oligotrophic KS surface water, nutrient limitation occurs throughout the year and all nutrients are lower than the thresholds. Chl is very low (averaged annual Chl $<$ 0.1 mg·m^{-3}) and has slight seasonal variation. In brief, Chl peaks generally occur in periods of relatively high nutrients, LE, temperature and Chl levels drop when nutrients or LE limitations occur. The diversity of Chl annual cycling can be mainly attributed to the changes in nutrient and light limitations. Since the variations of nutrients and LE are controlled by terrestrial inputs, water turbidity, vertical mixing, and oligotrophic water masses etc., which distribution usually associate with the terrain, the Chl annual cycle types tend to vary with water depth.

Although Chl variability is usually controlled by phytoplankton growth rate, the impact of phytoplankton loss cannot be ignored. Our results show that the LMC daily change rate is very small (about 0.01%–2.5% per day). In contrast, the division rate of phytoplankton in the ECSs has been reported at 0.26–2.29 d^{-1} (Choi et al., 2012; Sun and Song, 2009), which is at least one order of magnitude higher than the Chl daily changing rate. This tiny change in Chl daily rate implies a very close coupling between phytoplankton growth and loss. Behrenfeld and Boss (2014) pointed that the variation in Chl reflects the minor disequilibrium of phytoplankton division and loss rates; the latter is driven by accelerations and decelerations of the former. In th e ECSs, some studies reported that the grazing pressure can be much higher than the phytoplankton productivity in coastal water during summer and might make the Chl seasonal variation unstable (Tang et al., 2003; Zhang and Wang, 2000). However, due to a lack of large-scale grazing rate studies, the loss rate impact on phytoplankton distribution and seasonal cycles is still unknown.

5. Conclusions

In this study, a locally modified satellite Chl (LMC) dataset was generated, using ESA OC-CCI merged data and the nonlinear empirical relationship between nLw555 and the error of standard chlorophyll in the ECSs. As verified by the extensive in-situ data, LMC can provide a reasonable satellite view of Chl distribution, and is highly consistent with the ship-measured Chl results. We found that there are four annual Chl cycles in the ECSs and their distributions mainly correspond to water depth. Different annual Chl cycles can be explained by the changes in nutrients, temperature, and LE that are controlled by terrestrial inputs, ocean physical processes, and seasonal alternations. The highly dynamic and complex annual cycles of phytoplankton imply that the biogeochemical cycles in the ECSs cannot be completely revealed by the traditional four-season investigations. Therefore, full year and long-term in-situ observations should be strengthened and combined with data from buoys, satellites, and modeling studies. In addition, although LMC provides a more reasonable satellite Chl dataset in the ECSs, whether it can accurately reflect long-term trends in phytoplankton still needs further validation.

Conflicts of interest

The authors declare no financial conflicts of interest.

Acknowledgments

We thank ESA for providing the OC-CCI products. A portion of the in-situ data was derived from the SeaBASS in-situ database. We are

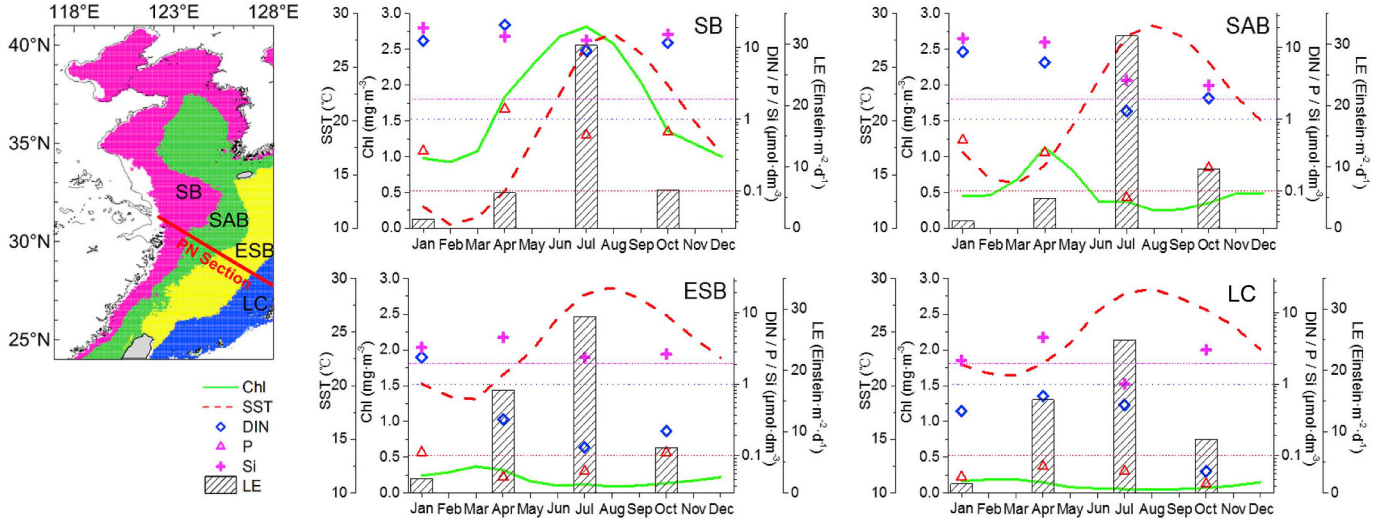

Fig. 6. Surface Chl and environmental factors including light exposure (LE) in the mixing layer, sea surface temperature (SST) and nutrients (DIN, P, and Si indicate dissolved inorganic nitrite, PO_4, and SiO_3 respectively) in summer bloom (SB), spring and autumn bloom (SAB), early spring bloom (ESB), and low chlorophyll (LC) regions in the PN section. The blue, red and purple dotted lines indicate the threshold values of DIN, PO_4 and SiO_3 respectively (DIN = 1 μmol·dm^{-3}, PO_4 = 0.1 μmol·dm^{-3}, and SiO_3 = 2 μmol·dm^{-3}), as suggested by Justić et al. (1995).

grateful to Prof. Joji Ishizaka and Dr. Xianqiang He for their valuable comments. Financial support for the study was provided by the National Key Research and Development Program of China (Grant No. 2016YFC1401601), the National Basic Research Program from the Ministry of Science and Technology of China [Grant Nos. 2010CB428904 and 2011CB409803], the Natural Science Foundation of China [Grant No. 41006101], the“908” project of China [Grant No. 908-01-04], the Project of State Key Laboratory of Satellite Ocean Environment Dynamics, China [Grant No. SOEDZZ1402] and the Second Institute of Oceanography Foundation, China [Grant No. JG1103].

Appendix A

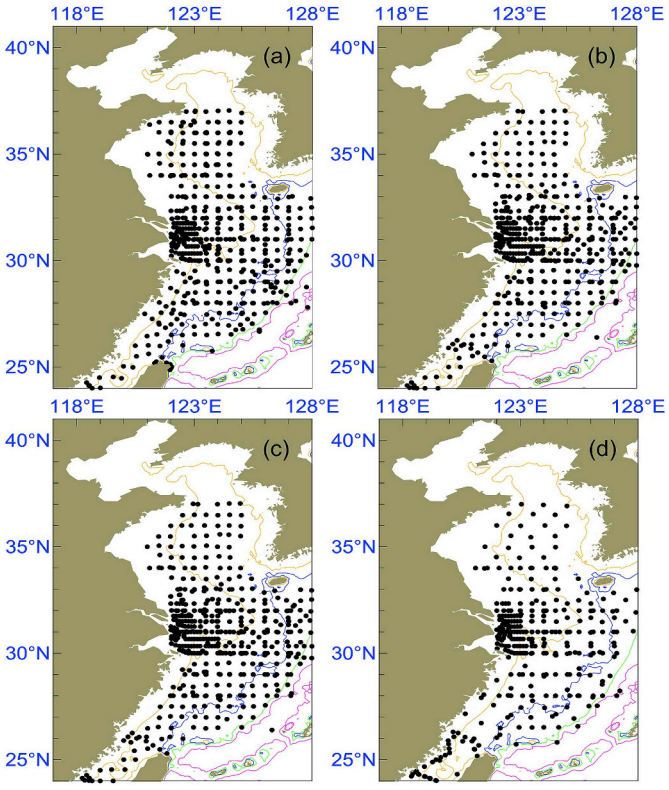

Fig. 1. The in-situ stations for making the integrated ship-measured Chl distributions. (a)spring, (b) summer, (c) autumn, (d) winter.

Table 1
Chl level and minimum/maximum season in different ship-measured studies.

Study area	Minimum Chl season/Maximum Chl season	Annual mean Chl($mg{\cdot}m^{-3}$)	Reference
BH	Winter/Summer	0.99	Fei et al. (1991)
BH	Winter/Summer	0.61	Lv et al. (1999)
BH	Winter/Summer or Spring	0.79	Tang, 2006
BH	Winter/Summer	1.94	Sun and Su, 2012
YS	Winter/Spring	–	Zhu et al. (1993)
YS	Winter/Spring	0.85	Ning et al. (1995) [a]
YS	Winter/Autumn	1.18	Sun and Su, 2012
ECS	Winter/Spring	0.47	Ning et al. (1995)
ECS	Early spring/Summer	0.95	Gong et al. (2003) [b]
ECS	Winter/Summer	1.70	Sun and Su (2012) [c]
Entire ECSs		1.05	

* The value was calculated from the seasonal mean Chl.
[a] The southern of YS.
[b] The continental shelf of ECS.
[c] The coastal and continental shelf of ECS.

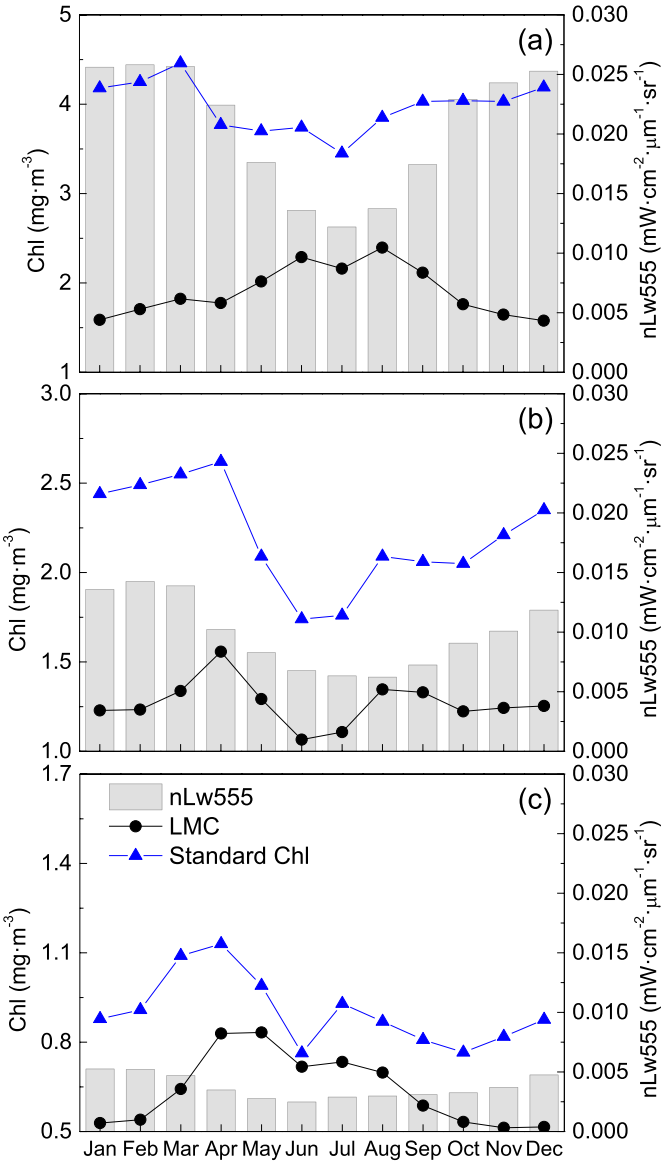

Fig. 2. Comparison between climatological monthly mean variations (1998–2013) of standard Chl, locally modified Chl (LMC), and normalized water-leaving radiance at 555 nm (nLw555) in **(a)** the Bohai Sea, **(b)** the Yellow Sea, and **(c)** the East China Sea.

Appendix B

(I) Procedures of Locally Modification of Standard Chl

The local modification was based on the empirical relationship between the error of standard Chl and water turbidity (555 nm normalized water-leaving radiance, nLw555). Firstly, to obtain a larger number of matches, we used 8-day-averaged satellite products instead of daily products to establish a preliminary correction function. The ratio of standard Chl to in-situ Chl (defined as f) was used to describe the standard Chl error and the averaged value of $Log_{10}(f)$ for each 0.1 increment of Log_{10}(nLw555) was collected in the 8-day matched dataset (A 0.1 increment was used to ensure that each increment included sufficient data points, whilst maintaining the statistical relationship between nLw555 and f.). According to the fitting result between $Log_{10}(f)$ and Log_{10}(nLw555) shown in Fig. 1a, we can use a fourth-order polynomial formulation to describe the relationship between f and nLw555 as follows:

$$Log_{10}(f) = -0.4122 \times Log_{10}^{4}(nLw555) + 0.4101 \times Log_{10}^{3}(nLw555) - 0.3810 \times Log_{10}^{2}(nLw555) + 0.2242 \times Log_{10}(nLw555) + 0.1929 \quad (5)$$

where the unit of nLw555 is $mW \cdot cm^{-2} \cdot \mu m^{-1} \cdot sr^{-1}$.

Secondly, a further correction was conducted after the preliminary modification of f by Eq. (1) for correcting the bias caused due to the use of the 8-d matched dataset. As Fig. 1b shows, the daily corrected Chl (C_{sat}/f, where C_{sat} and f are derived from daily matched data) and in-situ Chl ($C_{in\text{-}situ}$) have a significant linear correlation ($R^2 = 0.66$) and their relationship can be described via Eq. (2).

$$Log_{10}(C_{in\text{-}situ}) = 1.1108 \times Log_{10}(C_{sat}/f) + 0.0119 \quad (6)$$

Finally, with this correction, we were able to develop a method for local modification of the standard Chl product, by applying an exponential function converted from Eq. (2). See Eq. (3).

$$C_{LMC} = (C_{OC}/f)^{1.11} \quad (7)$$

where C_{LMC} is LMC, and C_{OC} is the daily standard Chl (calculated by the OC4 algorithm and NIR atmospheric correction). All Chl units are $mg \cdot m^{-3}$. Eq. (3) can be used to calculate f with the satellite-derived daily standard nLw555.

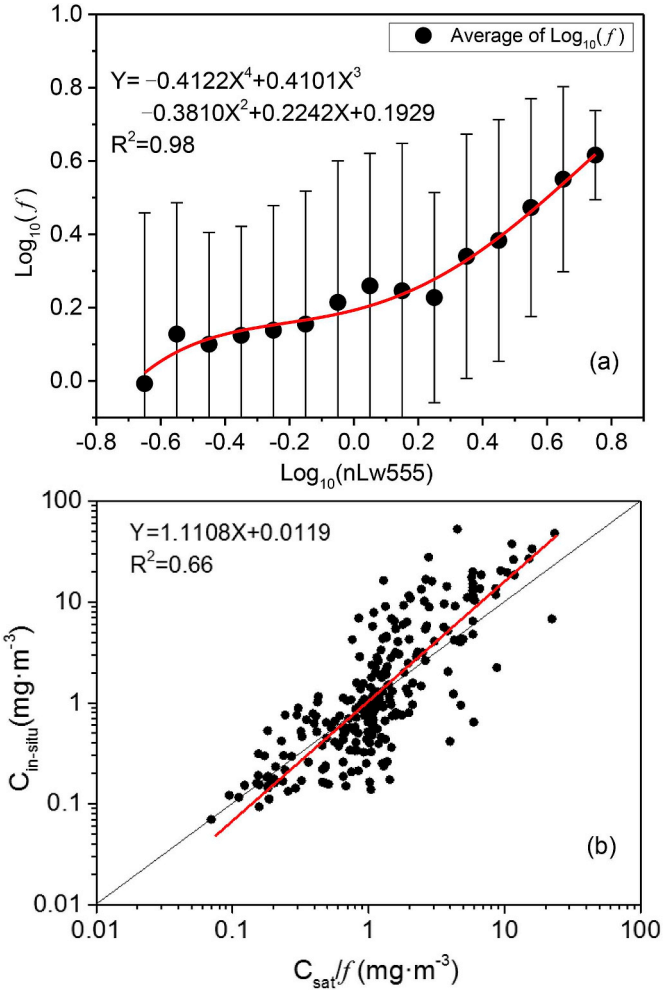

Fig. 3. (**a**) $Log_{10}(f)$ versus Log_{10}(nLw555). Bars indicate the standard deviation of f in each 0.1 increment of Log_{10}(nLw555), and the red curve is the fitted polynomial. The black dot is the average of $Log_{10}(f)$ for each 0.1 increment of Log_{10}(nLw555) and the error bar is the standard error of $Log_{10}(f)$ for each 0.1 increment of Log_{10}(nLw555). (**b**) preliminarily modified Chl (C_{sat}/f) versus daily matched in-situ Chl ($C_{in\text{-}situ}$). The black line is Y:X = 1:1, and the red line shows type II linear regression.

(II) Data collection and processing in the Fig. 6

In-situ data in the PN section data, including surface DIN, PO_4, and SiO_3 data from 84 stations collected during 2006–2007, come from "The China Sea Environment Integrated Survey and Assessment Project" and the online database of the Japan Meteorological Agency (http://www.data.jma.go.jp/gmd/kaiyou/db/vessel_obs/data-report/html/ship/ship_e.php). In each season, there are 7, 5, 5, and 4 stations for the SB, SAB, EAB, and LC regions respectively. The light exposure (LE) in the mixing layer for the four seasons was calculated using Eq. (4), where K was calculated using Secchi depth data and the mixing layer depth (MLD) was calculated by the vertical temperature gradient method. The source of the Secchi depth and temperature data is the same as that of the nutrient data. The daily surface photosynthetically available radiation (PAR) was derived from Moderate Resolution Imaging Spectroradiometer (MODIS-Aqua) daily L-3 products and was matched with the in-situ stations. The monthly Chlorophyll *a* (Chl) and sea surface temperature (SST) were derived from our LMC dataset and the Advanced Very High-Resolution Radiometer (AVHRR) products respectively.

References

Ahn, Y.H., Moon, J.E., Gallegos, S., 2001. Development of suspended particulate matter algorithms for ocean color remote sensing. Kor. J. Remote Sens. 17, 285–295.

Behrenfeld, M.J., Boss, E.S., 2014. Resurrecting the ecological underpinnings of ocean plankton blooms. Annu. Rev. Mar. Sci. 6, 167–194. https://doi.org/10.1146/annurev-marine-052913-021325.

Bian, C., Jiang, W., Greatbatch, R.J., Ding, H., 2013. The suspended sediment concentration distribution in the Bohai Sea, Yellow Sea and East China Sea. J. Ocean Univ. China 12, 345–354. https://doi.org/10.1007/s11802-013-1916-3.

Blondeau-Patissier, D., Gower, J., Dekker, A., Phinn, S., Brando, V., 2014. A review of ocean color remote sensing methods and statistical techniques for the detection, mapping and analysis of phytoplankton blooms in coastal and open oceans. Prog. Oceanogr. 123, 123–144 2014.

Chen, C.-T.A., 2009. Chemical and physical fronts in the Bohai, Yellow and East China seas. J. Mar. Syst. 78, 394–410. https://doi.org/10.1016/j.jmarsys.2008.11.016.

Chen, Y.L., Chen, H., Gong, G., Lin, Y., Jan, S., Takahashi, M., 2004. Phytoplankton production during a summer coastal upwelling in the East China Sea. Cont. Shelf Res. 24, 1321–1338.

Chen, S., Zhang, T., Hu, L., 2014. Evaluation of the NIR-SWIR atmospheric correction algorithm for MODIS-Aqua over the Eastern China Seas. Int. J. Rem. Sens. 35 (11–12), 4239–4251.

Choi, K.-H., Yang, E.J., Kim, D., Kang, H.-K., Noh, J.H., Kim, C.-H., 2012. The influence of coastal waters on distributions of heterotrophic protists in the northern East China Sea, and the impact of protist grazing on phytoplankton. J. Plankton Res. 34, 886–904. https://doi.org/10.1093/plankt/fbs046.

Dong, L., Guan, W., Chen, Q., Li, X., Liu, X., Zeng, X., 2011. Sediment transport in the Yellow Sea and East China Sea. Estuar. Coast. Shelf Sci. 93, 248–258. https://doi.org/10.1016/j.ecss.2011.04.003.

Falkowski, P.G., Raven, J.A., 2007. Aquatic photosynthesis, second ed. Princeton University Press, Princeton.

Falkowski, P.G., Barber, R.T., Smetacek, V., 1998. Biogeochemical controls and feedbacks on ocean primary production. Science 281, 200–206.

Fei, Z., Mao, X., Zhu, M., Li, B., Li, B., Guan, Y., Lv, R., 1991. The study of primary productivity in the Bohai Sea: chlorophyll a, primary productivity and potential fishery resources. Mar. Fish. Res. 12, 55–69 (In Chinese).

Foy, R.H., Gibson, C.E., 1993. The influence of irradiance, photoperiod and temperature on the growth kinetics of three planktonic diatoms. Eur. J. Phycol. 28, 203–212. https://doi.org/10.1080/09670269300650311.

Fu, M., Wang, Z., Li, Y., Li, R., Sun, P., Wei, X., Lin, X., Guo, J., 2009. Phytoplankton biomass size structure and its regulation in the Southern Yellow Sea (China): Seasonal variability. Cont. Shelf Res. 29, 2178–2194. https://doi.org/10.1016/j.csr.2009.08.010.

Gao, Y., Yang, T., Wang, Y., Yu, G., 2017. Fate of river-transported carbon in china: implications for carbon cycling in coastal ecosystems. Ecosyst. Health Sustain. 3, e01265. https://doi.org/10.1002/ehs2.1265.

Gohin, F., Druon, J.N., Lampert, L., 2002. A five channel chlorophyll concentration algorithm applied to SeaWiFS data processed by Seadas in coastal waters. Int. J. Rem. Sens. 23, 1639–1661.

Gohin, F., Loyer, S., Lunven, M., Labry, C., Froidefond, J.M., Delmas, D., Huret, M., Herbland, 2005. Satellite-derived parameters for biological modelling in coastal waters: Illustration over the eastern continental shelf of the bay of Biscay. Remote Sens. Environ. 95, 29–46. https://doi.org/10.1016/j.rse.2004.11.007.

Gong, G.-C., Chen, Y.-L.L., Liu, K.-K., 1996. Chemical hydrography and chlorophyll a distribution in the East China Sea in summer: implications in nutrient dynamics. Cont. Shelf Res. 16, 1561–1590.

Gong, G.-C., Wen, Y.-H., Wang, B.-W., Liu, G.-J., 2003. Seasonal variation of chlorophyll a concentration, primary production and environmental conditions in the subtropical East China Sea. Deep Sea Res. Part II Top. Stud. Oceanogr. 50, 1219–1236. https://doi.org/10.1016/S0967-0645(03)00019-5.

Gregg, W.W., Casey, N.W., 2004. Global and regional evaluation of the SeaWiFS chlorophyll data set. Remote Sens. Environ. 93, 463–479. https://doi.org/10.1016/j.rse.2003.12.012.

Han, J., 2008. Numerical study on the physical effect on phytoplankton bloom in the Yellow Sea. PhD thesis. Ocean University of China, Qingdao, China.

Han, B., Loisel, H., Vantrepotte, V., Mériaux, X., Bryère, P., Ouillon, S., Dessailly, D., Xing, Q., Zhu, J., 2016. Development of a semi-analytical algorithm for the retrieval of Suspended Particulate Matter from remote sensing over clear to very turbid waters. Rem. Sens. 8 (3), 211. https://doi.org/10.3390/rs8030211.

Hao, J., Chen, Y., Wang, F., Lin, P., 2012. Seasonal thermocline in the China Seas and northwestern Pacific Ocean. J. Geophys. Res. Oceans 117. https://doi.org/10.1029/2011JC007246.

He, X., Bai, Y., Pan, D., Tang, J., Wang, D., 2012. Atmospheric correction of satellite ocean color imagery using the ultraviolet wavelength for highly turbid waters. Optic Express 20 (18), 20754–20770.

He, X., Bai, Y., Pan, D., Chen, A., Chen, Q., Wang, D., Gong, F., 2013a. Satellite views of the seasonal and inter-annual variability of phytoplankton blooms in the eastern China seas over the past 14 yr (1998-2011). Biogeosciences 10, 4721–4739.

He, X., Bai, Y., Pan, D., Huang, N., Dong, X., Chen, J., Chen, A., Cui, Q., 2013b. Using geostationary satellite ocean color data to map the diurnal dynamics of suspended particulate matter in coastal waters. Remote Sens. Environ. 133, 225–239.

Hu, J., Wang, X.H., 2016. Progress on upwelling studies in the China seas: upwelling studies in the China Seas. Rev. Geophys. 54, 653–673. https://doi.org/10.1002/2015RG000505.

Huang, D., Zhang, T., Zhou, F., 2010. Sea-surface temperature fronts in the Yellow and East China Seas from TRMM microwave imager data. Deep Sea Res. Part II Top. Stud. Oceanogr. 57, 1017–1024. https://doi.org/10.1016/j.dsr2.2010.02.003.

Ichikawa, H., Beardsley, R.C., 2002. The current system in the Yellow and East China Seas. J. Oceanogr. 58, 77–92.

IOCCG, 2000. Remote sensing of ocean colour in coastal, and other optically complex, waters. In: Sathyendranath, S. (Ed.), Reports of the international ocean colour coordinating group, No. 3. IOCCG, Dartmouth, Canada, pp. 1–140.

Jin, J., Liu, S.M., Ren, J.L., Liu, C.G., Zhang, J., Zhang, G.L., Huang, D.J., 2013. Nutrient dynamics and coupling with phytoplankton species composition during the spring blooms in the Yellow Sea. Deep Sea Res. Part II Top. Stud. Oceanogr. 97, 16–32. https://doi.org/10.1016/j.dsr2.2013.05.002.

Johnson, R., Strutton, P.G., Wright, S.M., McMinn, A., Meiners, K.M., 2013. Three improved satellite chlorophyll algorithms for the Southern Ocean. J. Geophys. Res.: Oceans 118, 3694–3703. https://doi.org/10.1002/jgrc.20270.

Justić, D., Rabalaisb, N.N., Turnerb, E.R., Dortchb, Q., 1995. Changes in nutrient structure of river-dominated coastal waters: Stoichiometric nutrient balance and its consequences. Estuar. Coast Shelf Sci. 40, 339–356.

Kiyomoto, Y., Iseki, K., Okamura, K., 2001. Ocean color satellite imagery and shipboard measurements of chlorophyll a and suspended particulate matter distribution in the East China Sea. J. Oceanogr. 57, 37–45.

Li, G., Qiao, L., Dong, P., Ma, Y., Xu, J., Liu, S., Liu, Y., Li, J., Li, P., Ding, D., Wang, N., Olusegun, D., Liu, L., 2016. Hydrodynamic condition and suspended sediment diffusion in the Yellow Sea and East China Sea. Journal of Geophysical Research: Oceans 121, 6204–6222.

Li, G., Talmy, D., Campbell, D.A., 2017. Diatom growth responses to photoperiod and light are predictable from diel reductant generation. J. Phycol. 53, 95–107. https://doi.org/10.1111/jpy.12483.

Liu, D.Y., Wang, Y.Q., 2013. Trends of satellite derived chlorophyll-a (1997-2011) in the Bohai and Yellow Seas, China: Effects of bathymetry on seasonal and inter-annual patterns. Prog. Oceanogr. 116, 154–166.

Liu, J.P., Li, A.C., Xu, K.H., Velozzi, D.M., Yang, Z.S., Milliman, J.D., DeMaster, D.J., 2006. Sedimentary features of the Yangtze River-derived along-shelf clinoform deposit in the East China Sea. Cont. Shelf Res. 26, 2141–2156. https://doi.org/10.1016/j.csr.2006.07.013.

Lv, R., Xia, B., Li, B., Fei, Z., 1999. The fluctuations of primary productivity in Bohai Sea waters over ten years. J. Oceanogr. Huanghai Bohai Seas 17 (3), 80–86 (in Chinese with English abstract).

Ng, A.Y., Jordan, M.I., Weiss, Y., 2001. On Spectral Clustering: Analysis and an algorithm. pp. 8.

Nicklisch, A., Shatwell, T., Köhler, J., 2008. Analysis and modelling of the interactive effects of temperature and light on phytoplankton growth and relevance for the spring bloom. J. Plankton Res. 30, 75–91.

Ning, X., Liu, Z., Shi, J., 1995. Primary production and estimation of potential fish catch in the Bohai Sea,Yellow Sea and East China Sea. 1995. Acta Oceanol. Sin. 17 (3), 72–84 (in Chinese with English abstract).

Ning, X., Liu, Z., Cai, Y., Chai, F., 1998. Physicobiological oceanographic remote sensing of the ECS: Satellite and in-situ observations. J. Geophys. Res. 103 (C10), 21623–21636.

Ning, X., Liu, Z., Cai, Y., 2000. A review on primary production studies for China seas in the past 20 years. Donghai Mar. Sci. 18 (3), 13–20.

Ning, X., Shi, J., Cai, Y., Liu, C., 2004. Biological productivity front in the Changjiang Estuary and the Hangzhou Bay and its ecological effects. Acta Oceanol. Sin. 26 (6),

96–106 (in Chinese with English abstract).
O'Reilly, J.E., Maritorena, S., Siegel, D.A., O'Brien, M.C., Toole, D., Mitchell, B.G., Kahru, M., Chavez, F.P., Strutton, P., Cota, G.F., Hooker, S.B., McClain, C.R., Carder, K.L., Muller-Karger, F., Harding, L., Magnuson, A., Phinney, D., Moore, G.F., Aiken, J., Arrigo, K.R., Letelier, R., Culver, M., 2000. Ocean Color Chlorophyll a Algorithms for SeaWiFS, OC2 and OC4: Version 4 15.
Pan, Y., Xu, D., Xu, J., 1987. The structure of fronts and their causes in the coastal upwelling area off Zhejiang. Acta Oceanol. Sin. 6, 177–189.
Qiao, L., Zhong, Y., Wang, N., Zhao, K., Huang, L., Wang, Z., 2016. Seasonal transportation and deposition of the suspended sediments in the Bohai Sea and Yellow Sea and the related mechanisms. Ocean Dynam. 66, 751–766.
Reygondeau, G., Longhurst, A., Martinez, E., Beaugrand, G., Antoine, D., Olivier, M., 2013. Dynamic biogeochemical provinces in the global ocean. Glob. Biogeochem. Cycles 27 (4), 1046–1058. https://doi.org/10.1002/gbc.20089.
Shi, J., Malik, J., 2000. Normalized Cuts and Image Segmentation. IEEE Trans. Pattern Anal. Mach. Intell. 22, 18.
Shi, W., Wang, M., 2010. Satellite observations of the seasonal sediment plume in central East China Sea. J. Mar. Syst. 82, 280–285.
Shi, W., Wang, M., 2012. Satellite views of the Bohai Sea, Yellow Sea, and East China Sea. Prog. Oceanogr. 104, 30–45. https://doi.org/10.1016/j.pocean.2012.05.001.
Siegel, D.A., Wang, M., Maritorena, S., 2000. Atmospheric correction of satellite ocean color imagery: The black pixel assumption. Appl. Optic. 39 (21), 3582–3591.
Siswanto, E., Tang, J., Yamaguchi, H., Ahn, Y.-H., Ishizaka, J., Yoo, S., Kim, S.-W., Kiyomoto, Y., Yamada, K., Chiang, C., Kawamura, H., 2011. Empirical ocean-color algorithms to retrieve chlorophyll-a, total suspended matter, and colored dissolved organic matter absorption coefficient in the Yellow and East China Seas. J. Oceanogr. 67, 627–650. https://doi.org/10.1007/s10872-011-0062-z.
Sokal, R., Rohlf, F., 1995. Biometry: The principles and practice of statistics in biological research, third ed. W. H. Freeman.
Song, H., Zhang, X., Wang, B., Sun, X., Wang, X., Xin, M., 2014. Bottom-up and top-down controls of the phytoplankton standing stock off the Changjiang Estuary. Acta Oceanol. Sin. (in Chinese) 36 (8), 91–100. https://doi.org/10.3969/j. issn, 0253-.4193.2014.08.010.
Song, C., Wang, G., Sun, X., Chang, R., Mao, T., 2016. Control factors and scale analysis of annual river water, sediments and carbon transport in China. Sci. Rep. 6. https://doi.org/10.1038/srep25963.
Sun, J., Song, S., 2009. The study of phytoplankton growth and micro-zooplankton herbivory during spring phytoplankton bloom period in the East China Sea. Acta Ecol. Sin. 29, 6429–6438.
Sun, S., Su, J. (Eds.), 2012. Regional oceanography of China seas-biological oceanography. Ocean Press, Beijing (in Chinese).
Tang, Q. (Ed.), 2006. Living Marine Resources and Inhabiting Environment in the Chinese EEZ. Science Press, Beijing (in Chinese).
Tang, Q. (Ed.), 2012. Regional oceanography of China seas-fisheries oceanography. Ocean Press, Beijing (in Chinese).
Tang, D.L., Ni, I.H., Müller-Karger, F.E., Liu, Z.J., 1998. Analysis of annual and spatial patterns of CZCS-derived pigment concentration on the continental shelf of China. Cont. Shelf Res. 18, 1493–1515.
Tang, Q., Jin, X., Wang, J., Zhuang, Z., Cui, Y., Meng, T., 2003. Decadal-scale variations of ecosystem productivity and control mechanisms in the Bohai Sea. Fish. Oceanogr. 12, 223–233.
Volpe, G., Santoleri, R., Vellucci, V., Ribera d'Alcala, M., Marullo, S., D'Ortenzio, F., 2007. The colour of the Mediterranean Sea: global versus regional bio-optical algorithms evaluation and implication for satellite chlorophyll estimates. Remote Sens. Environ 107, 625–638.
von Luxburg, U., 2007. A tutorial on spectral clustering. Stat. Comput. 17, 395–416. https://doi.org/10.1007/s11222-007-9033-z.
Wang, M., 2007. Remote sensing of the ocean contributions from ultraviolet to near-infrared using the shortwave infrared bands: simulations. Appl. Opt. 46, 1535. https://doi.org/10.1364/AO.46.001535.
Wang, B., Wang, X., 2007. Chemical hydrography of coastal upwelling in the East China Sea. Chin. J. Oceanol. Limnol. 25, 16–26. https://doi.org/10.1007/s00343-007-0016-x.
Wang, B., Wang, X., Zhan, R., 2003. Nutrient conditions in the Yellow Sea and the East China Sea. Estuar. Coast Shelf Sci. 58, 127–136.
Wang, Y., Liu, R., Su, J., 2013. China's Marine Geography. Science Press, Beijing.
Wang, H., Dai, M., Liu, J., Kao, S.-J., Zhang, C., Cai, W.-J., Wang, G., Qian, W., Zhao, M., Sun, Z., 2016. Eutrophication-Driven Hypoxia in the East China Sea off the Changjiang Estuary. Environ. Sci. Technol. 50, 2255–2263. https://doi.org/10.1021/acs.est.5b06211.
Wong, G.T.F., Gong, G.-C., Liu, K.-K., Pai, S.-C., 1998. 'Excess Nitrate' in the East China Sea. Estuar. Coast. Shelf Sci. 46, 411–418. https://doi.org/10.1006/ecss.1997.0287.
Yamaguchi, H., Kim, H.-C., Son, Y.B., Kim, S.W., Okamura, K., Kiyomoto, Y., Ishizaka, J., 2012. Seasonal and summer interannual variations of SeaWiFS chlorophyll a in the Yellow Sea and East China Sea. Prog. Oceanogr. 105, 22–29. https://doi.org/10.1016/j.pocean.2012.04.004.
Yamaguchi, H., Ishizaka, J., Siswanto, E., Baek Son, Y., Yoo, S., Kiyomoto, Y., 2013. Seasonal and spring interannual variations in satellite-observed chlorophyll-a in the Yellow and East China Seas: New datasets with reduced interference from high concentration of resuspended sediment. Cont. Shelf Res. 59, 1–9. https://doi.org/10.1016/j.csr.2013.03.009.
Yang, S.Y., Jung, H.S., Lim, D.I., Li, C.X., 2003. A review on the provenance discrimination of sediments in the Yellow Sea. Earth Sci. Rev. 63, 93–120.
Zhang, W., Wang, R., 2000. Summertime ciliate and copepod nauplii distributions and micro-zooplankton herbivorous activity in the Laizhou Bay, Bohai Sea, China. Estuar. Coast. Shelf Sci. 51, 103–114. https://doi.org/10.1006/ecss.2000.0644.
Zhang, J., Liu, S.M., Ren, J.L., Wu, Y., Zhang, G.L., 2007. Nutrient gradients from the eutrophic Changjiang (Yangtze River) Estuary to the oligotrophic Kuroshio waters and re-evaluation of budgets for the East China Sea Shelf. Prog. Oceanogr. 74, 449–478. https://doi.org/10.1016/j.pocean.2007.04.019.
Zhou, F., Xuan, J., Huang, D., Liu, C., Sun, J., 2013. The timing and the magnitude of spring phytoplankton blooms and their relationship with physical forcing in the central Yellow Sea in 2009. Deep Sea Res. Part II Top. Stud. Oceanogr. 97, 4–15. https://doi.org/10.1016/j.dsr2.2013.05.001.
Zhu, M., Mao, X.H., Lv, R.H., Sun, M., 1993. Chlorophyll a and primary productivity in the Yellow Sea. J. Oceanogr. Huanghai Bohai Seas 11, 38–51 (in Chinese).
Zhu, Z.-Y., Ng, W.-M., Liu, S.-M., Zhang, J., Chen, J.-C., Wu, Y., 2009. Estuarine phytoplankton dynamics and shift of limiting factors: A study in the Changjiang (Yangtze River) Estuary and adjacent area. Estuar. Coast. Shelf Sci. 84, 393–401. https://doi.org/10.1016/j.ecss.2009.07.005.